JOURNAL OF GEOPHYSICAL RESEARCH, VOL. 106, NO. D15, PAGES 17,237–17,252, AUGUST 16, 2001

A conceptual model of the dehydration of air due to freeze-drying by optically thin, laminar cirrus rising slowly across the tropical tropopause

Eric J. Jensen, Leonhard Pfister, Andrew S. Ackerman, and Azadeh Tabazadeh
NASA Ames Research Center, Moffett Field, California

Owen B. Toon
University of Colorado, Laboratory for Atmospheric and Space Physics, Boulder, Colorado

Abstract.

In this study, we use a cloud model to simulate dehydration which occurs due to formation of optically thin, laminar cirrus as air rises slowly across the tropopause. The slow ascent and adiabatic cooling, which balances the radiative heating near the tropopause, drives nucleation of a very small number of ice crystals ($< 1\ L^{-1}$). These crystals grow rapidly and sediment out within a few hours. The clouds never become optically thick enough to be visible from the ground. The ice crystal nucleation and growth prevents the relative humidity with respect to ice (RHI) from rising more than a few percent above the threshold for ice nucleation ($RHI_{nuc} \simeq 110$–160%, depending upon the aerosol composition); hence, laminar cirrus can limit the mixing ratio of water vapor entering the stratosphere. However, the ice number densities are too low and their sedimentation is too rapid to allow dehydration of the air from RHI_{nuc} down to saturation (RHI = 100%). The net result is that air crosses the tropopause with water vapor mixing ratios about 1.1 to 1.6 times the ice saturation mixing ratio corresponding to the tropopause temperature, depending on the threshold of ice nucleation on aerosols in the tropopause region. If the cross-tropopause ascent rate is larger than that calculated to balance radiative heating (0.2 cm s^{-1}), then larger ice crystal number densities are generated, and more effective dehydration is possible (assuming a fixed temperature). The water vapor mixing ratio entering the stratosphere decreases with increasing ascent rate (approaching the tropopause ice saturation mixing ratio) until the vertical wind speed exceeds the ice crystal terminal velocity (about 10 cm s^{-1}). More effective dehydration can also be provided by temperature oscillations associated with wave motions. The water vapor mixing ratio entering the stratosphere is essentially controlled by the tropopause temperature at the coldest point in the wave. Hence, the efficiency of dehydration at the tropopause depends upon both the effectiveness of upper tropospheric aerosols as ice nuclei and the occurrence of wave motions in the tropopause region. In situ humidity observations from tropical aircraft campaigns and balloon launches over the past several years have provided a few examples of ice-supersaturated air near the tropopause. However, given the scarcity of data and the uncertainties in water vapor measurements, we lack definitive evidence that air entering the stratosphere is supersaturated with respect to ice.

1. Introduction

Water vapor is the dominant greenhouse gas in the Earth's atmosphere. Even though the water vapor concentrations are relatively low above the tropopause, the water in the lower stratosphere is radiatively important in the infrared due to the low temperatures [*Clough et al.*, 1992]. Water vapor is also critical for chemical processes in the stratosphere. The composition of sulfate aerosols and the formation of polar stratospheric clouds are controlled by water vapor concentration [*Hamill et al.*, 1977; *Toon et al.*, 1989a]. These aerosol and cloud particles, in turn, play key roles in destruction of stratospheric ozone [*Solomon et al.*, 1986]. Motivated by the importance of water vapor to stratospheric processes,

Paper number 2000JD900649.
0148-0227/01/2000JD900649$09 00

considerable effort has been focused on understanding the stratospheric water budget.

The dominant sources of water vapor in the stratosphere are upward transport of relatively humid air across the cold tropical tropopause and oxidation of methane in the middle stratosphere. These sources are thought to contribute roughly equally to the 5–6 ppmv of water vapor present in the middle stratosphere [*Dessler,* 1998]. In the tropical lower stratosphere, air has recently entered the stratosphere from the troposphere, and methane oxidation has not yet contributed to the water vapor concentration. In this region the water vapor mixing ratio is very low (about 2.5–4 ppmv [*Hintsa et al.,* 1999]). Invariably, the explanation given for these low water vapor mixing ratios is that as air crosses the cold tropical tropopause it is "freeze-dried" to the low ice saturation mixing ratios there. (In this paper we define the tropopause as the height of the temperature minimum, since this is the critical location for the dehydration processes. Also, since we are focusing on the extremely cold tropical tropopause in this paper, all saturations and humidities discussed are with respect to ice.) Analyses of the stratospheric water vapor budget generally compare the ice saturation water vapor mixing ratio corresponding to the observed tropopause temperatures to the observed water vapor mixing ratios in the lower stratosphere [e.g., *Dessler,* 1998; *Newell and Gould-Stewart,* 1981; *Weinstock et al.,* 1995]. There is little doubt that the water mixing ratio in the lower tropical stratosphere must, to some degree, be controlled by the tropopause temperature. However, the details of how air enters the stratosphere and how dehydration occurs are not well understood.

A simple two-dimensional (latitude-height) view of the atmosphere would imply slow transport of air from the troposphere into the stratosphere in the tropics [*Brewer,* 1949]. The dehydration could then be explained by widespread formation of ice clouds at the tropopause. This simplified view was previously discounted since ubiquitous, extensive cirrus were not observed near the tropical tropopause [*Robinson,* 1980]. Also, it was argued that dehydration of air to the observed stratospheric water vapor mixing ratios can only occur in particular regions of the tropics where the tropopause temperatures are low enough [*Newell and Gould-Stewart,* 1981]. Hence, it was argued that most of the flux of air into the stratosphere occurs in the "stratospheric fountain" regions of the western Pacific, northern Australia, and India. Further, it was suggested that much of the flux of air into the stratosphere and the dehydration is attributable to direct injection by strong convective systems that overshoot the tropopause [*Robinson,* 1980; *Danielsen,* 1993]. *Sherwood and Dessler*, [2000] recently presented a mechanism for dehydration in vigorous convective overshoots. However, the issue of how air enters the stratosphere (via direct, localized convective injection or slow, widespread ascent) remains unresolved.

Recent lidar observations have shown that optically thin, laminar cirrus are very common near the tropical tropopause [e.g., *McFarquhar et al.,* 2000; *Winker and Trepte,* 1998]. These clouds provide a possible mechanism for dehydration associated with large-scale ascent across the tropopause. The conceptual model of air rising slowly across the tropopause throughout the tropics is supported by the high relative humidities [*Jensen et al.,* 1999] and high frequency of laminar, optically thin cirrus occurrence [*Wang et al.,* 1996] throughout the tropics near the tropopause. Also, radiative transfer calculations suggest that under clear-sky conditions, the tropopause region (14–20 km) is radiatively heated. On average, the heating rates of the order of 0.5 K d^{-1} (see calculations discussed below) must be balanced by adiabatic cooling associated with a mean vertical ascent of a few millimeters per second.

Recent in situ measurements in the upper troposphere have shown that substantial supersaturations with respect to ice can exist without nucleation of ice crystals [*Heymsfield et al.,* 1998; *Jensen et al.,* 1998a; *Gierens et al.,* 1999]. Clear-sky relative humidities with respect to ice as high as 160% were observed. The field observations of ice supersaturation are consistent with recent laboratory studies which have shown that ice supersaturations of about 60% are required to initiate homogeneous freezing of sulfate aerosols at upper tropospheric temperatures [*Koop et al.,* 1998]. Hence, the assumption that air entering the lower stratosphere will necessarily be dehydrated to the saturation mixing ratio as it crosses the tropopause is suspect. It is possible that air crossing the tropical tropopause may be supersaturated with respect to ice, thus allowing more water vapor to enter the stratosphere than assumed in the earlier assessments.

The efficiency of dehydration by cloud formation depends upon several coupled factors including the number of ice crystals nucleated, how large the crystals grow, the fall speed of the ice crystals, and cloud lifetimes [*Jensen et al.,* 1996]. A range of scenarios are possible: If the ice crystals do not grow large enough to fall relative to the rising air, then they will simply sublimate as the air rises into warmer regions in the stratosphere, and no net dehydration will occur. If enough ice crystals form to deplete the vapor in excess of saturation, and the crystals fall rapidly, then the water vapor mixing ratio will be effectively reduced to the tropopause saturation mixing ratio. A third possibility is that ice nucleation and growth prevents the relative humidity with respect to ice (RHI) from increasing more than a few percent beyond the critical value for initiation of ice nucleation (RHI_{nuc}), but relatively few ice crystals nucleate and they fall out before the RHI can be reduced substantially below RHI_{nuc}. Of course, the relative humidity of air entering the stratosphere may range from 100% to RHI_{nuc}, depending on the number density of ice crystals nucleated.

In a previous study, we modeled the potential for dehydration due to ice cloud formation driven by gravity waves at the tropopause [*Jensen et al.,* 1996]. In this study, we use a microphysical-dynamical model to evaluate the potential for freeze-drying of air rising slowly across the tropical tropopause. The sensitivity of the water vapor mixing ratio entering the stratosphere to ascent rate and RHI_{nuc} is analyzed with one-dimensional simulations, and the influence of wave-driven temperature oscillations on the cloud formation and dehydration processes is evaluated with two-dimensional (2-D) simulations. In addition, we have gathered in situ observations of humidity from past aircraft campaigns to search for evidence of supersaturation near the tropical tropopause.

2. Simulations of Freeze-Drying Driven by Slow Ascent

To simulate the formation of ice clouds in slowly rising air, we use a detailed microphysical model previously used in several ice cloud studies [e.g., *Jensen et al.,* 1998]. Two particle types are included: sulfate solution (H_2SO_4/H_2O) haze particles and ice crystals. For each particle type, 40 radius bins are included spanning the ranges 0.04 – 3.2 μm for sulfate aerosols, and 0.2 – 66 μm for ice crystals. For the sulfate aerosols, we assume a lognormal size distribution with a number density of 1000 cm^{-3}, mode radius of 0.04 μm, and standard deviation of 1.2 based on in situ measurements in the tropical upper troposphere [*Brock et al.,* 1995; *Clarke,* 1992]. As previous modeling studies have shown [e.g., *Jensen and Toon,* 1994], the ice crystal number density generated by homogeneous freezing of sulfate aerosols is very insensitive to the aerosol size distribution; sensitivity tests showed that changing the size distribution had negligible effects on the model results. A vertical domain extending from 14 to 19 km is used, with a vertical resolution of 20 m.

Ice crystal growth rates and sedimentation rates are calculated as described by *Jensen et al.* [1994]. A deposition coefficient (or mass accommodation coefficient) of unity is assumed. For calculating rates of ice nucleation in sulfate aerosols, we use the expressions recommended by *Tabazadeh et al.* [2000]. This parameterization is designed to match laboratory measurements of sulfuric acid solution aerosol freezing [*Koop et al.,* 1998]. The formulation predicts aerosol freezing at ice supersaturations of about 60% at typical tropical tropopause temperatures ($\leq$ -75°C). The primary difference between the model used here and that used in our earlier study [*Jensen et al.,* 1996] is that we previously used an ice nucleation model that predicted sulfate aerosol freezing at much smaller ice supersaturations (<10%).

Longwave and shortwave radiative fluxes and heating rates are calculated with a two-stream code [*Toon et al.,* 1989b] coupled to the model. Ice crystal single-scattering properties are calculated with a Mie scattering code. The combined microphysics-radiative transfer model allows us to simulate all of the processes critical for this problem: ice nucleation, crystal deposition growth and sublimation, sedimentation, radiative heating, and vertical advection. As we will show, the clouds which form in slowly rising air at the tropical tropopause have very low ice water contents (< 10 μg m^{-3}). As a result, the radiative and latent heating in the clouds do not drive thermal instability or substantial secondary motions in the cloud. A few 2-D simulations were run with an eddy-resolving dynamical model to verify our assertion that convective motions are not generated in the clouds. We used a 50 km horizontal grid with 50 m grid spacing and periodic horizontal boundary conditions. No significant secondary circulations were generated due to the cloud radiative heating. Hence, we use a 1-D model for the simulations described below.

The initial temperature, water vapor, relative humidity, and vertical wind speed profiles used in the model are shown in Figure 1. The thermal structure is specified based on ER-2 temperature profiles from the Stratosphere-Troposphere Exchange Project (STEP) [*Russell et al.,* 1993]. The initial water vapor mixing ratio profile is specified such that the RHI is near 100% at the tropopause. The vertical motion is specified such that the adiabatic cooling rate equals the radiative heating rate at each vertical level. The calculated daytime radiative heating rate is negative (cooling) below about 14.7 km, and positive (heating) above this level, with a maximum radiative heating rate of about 0.3 K d^{-1} near the tropopause. The vertical wind speed profile required to balance this heating crosses zero at 14.7 km and has a maximum value of $w = 0.2$ cm s^{-1} at the tropopause. The sharp discontinuities in w at 16.7 and 17 km are associated with the discontinuities in temperature lapse rate at these heights. At each time step in the simulation, we calculate the radiative heating rate (including cloud radiative heating) and recalculate the vertical wind speed accordingly. With this imposed vertical motion, the temperature in the simulation remains approximately constant with time.

The calculated radiative heating rate depends upon several assumptions, including surface temperature, water vapor concentration profile, ozone mixing ratio profile, and the temperature profile. Given uncertainties in these parameters, a reasonable range of peak heating rates is about 0.1 – 1 K d^{-1}, corresponding to a range in the peak vertical wind speed of about 0.06 – 0.6 cm s^{-1}. Given the insensitivity of our results to w in this range discussed below, the uncertainty in radiative heating rate should not affect our conclusions.

The vertical eddy diffusion coefficient is set to 10^4 cm^2-s^{-1} such that diffusion has very little impact on the simulation. At the bottom of the model where $w \lesssim 0$ and at the top of the model where $w > 0$, we allow water vapor and particles to advect across the model boundaries. Advection of particles and water vapor is treated

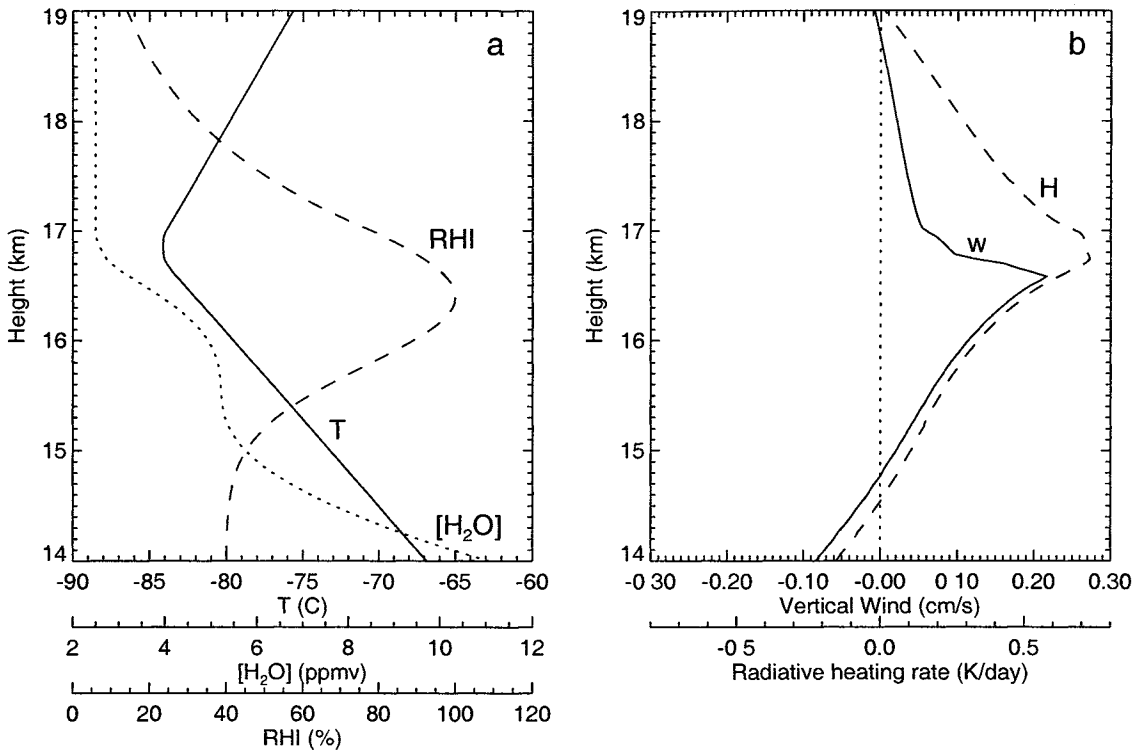

Figure 1. Simulation initial conditions. (a) Height profiles of temperature, relative humidity with respect to ice (RHI), and water vapor mixing ratio. (b) Height profiles of radiative heating rate (dashed) and the imposed vertical wind velocity (solid) specified such that the adiabatic cooling balances the radiative heating.

assuming that any vertical divergence/convergence is balanced by horizontal convergence/divergence. This assumption is consistent with holding the atmospheric density profile constant with time.

If we allow the water vapor profile to evolve due to advection alone (i.e, without allowing ice nucleation), then the imposed ascent above 14.7 km results in increasing humidity with time due to the negative gradient in water vapor mixing ratio with height. Below 14.7 km the subsidence drives the water vapor mixing ratio downward. After several days, air with unrealistically high water vapor mixing ratios exceeding 5 ppmv would be transported into the stratosphere if no clouds formed.

Results for the baseline simulation including ice nucleation are shown in Plate 1. When the RHI exceeds about 160% (at about 4 days), the sulfate aerosols begin to freeze, resulting in nucleation of ice crystals. The ice number densities are very low (no larger than 0.5 L^{-1}) due to the large barrier to nucleation of ice in aerosols and the very slow cooling rates. As a result, the crystals grow to radii of 10–25 μm, with resulting fall speeds of about 1.7–10 cm s^{-1}. The crystals fall out of the supersaturated region near the tropopause within a few hours. As soon as the ice crystals sediment out of the tropopause region, the RHI builds up again until another nucleation event occurs. After about 70 hours, new ice crystals nucleate as fast as they are depleted by sedimentation. The peak zenith optical depth in the cloud gets no larger than about 3 x 10^{-4}, which is well below the threshold for cloud visibility (approximately 0.03 [*Sassen et al.* 1989]). The ice nucleation and growth prevents the RHI from substantially exceeding the threshold for ice nucleation ($RHI_{nuc} \simeq 160\%$). However, owing to the low ice number density and rapid sedimentation, the crystal growth does not deplete the vapor in excess of saturation. The net result is that air enters the stratosphere with a water vapor concentration about 1.6 times the tropopause saturation water vapor mixing ratio. The buildup of water at about 15.5 km apparent in the bottom graph of Plate 1 is caused by sublimation of falling ice crystals.

As has been demonstrated in previous modeling studies [*Jensen and Toon,* 1994; *DeMott et al.,* 1997], the ice number density generated by homogeneous freezing of sulfate aerosols increases rapidly with increasing vertical wind speed. Hence, one would expect that with higher ascent rates, more ice crystals would nucleate, and the clouds might more effectively dehydrate the air. To examine this sensitivity, we have run a series of simulations with the vertical wind speed profile increased by factors ranging from 2 to 200 (corresponding to peak vertical wind speeds ranging from 0.4 to 20 cm s^{-1}). In these simulations, we held the temperature profile fixed so we could isolate the impact of the cloud on water va-

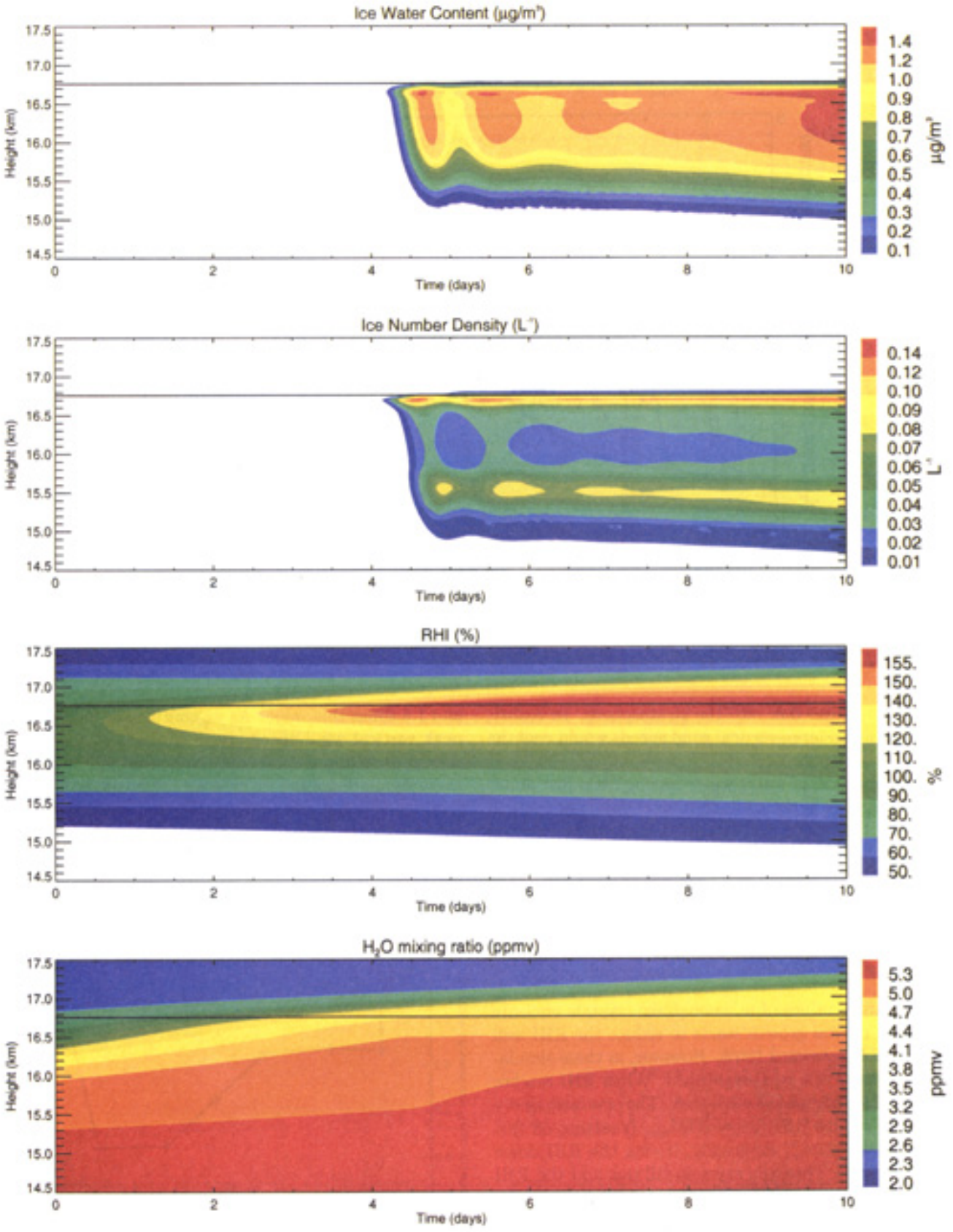

Plate 1. Results from the baseline simulation with $RHI_{nuc} = 160\%$. The graphs (from top to bottom) show ice water content, ice crystal number density, RHI, and H_2O mixing ratio versus time and height. The horizontal line at 16.75 km indicates the tropopause location. Sporadic ice nucleation and growth limits the RHI at the tropopause to about 160%, but the ice number densities are too low to reduce RHI down to near 100%.

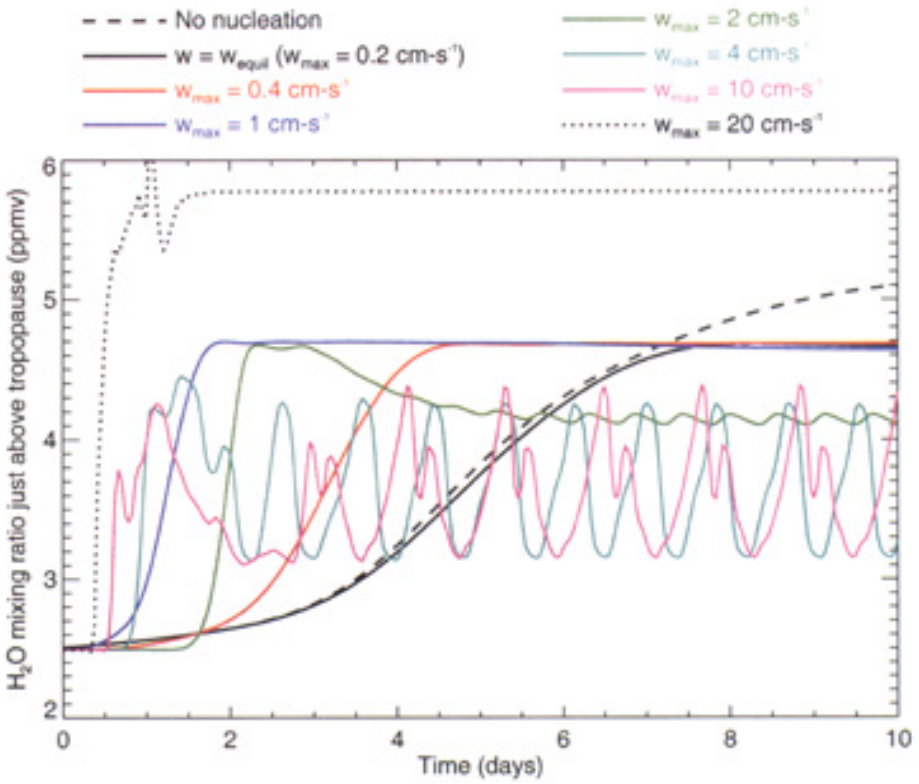

Plate 2. The water vapor mixing ratio just above the tropopause is plotted versus time from simulations with peak vertical wind speeds ranging from 0.2 to 20 cm s^{-1}. The temperature profile was held constant in these simulations.

por mixing ratio flux into the stratosphere. In reality, such sustained large vertical wind speeds would cool the tropopause region.

The evolution of water vapor mixing ratio just above the tropopause in these simulations is shown in Plate 2. Figure 2 shows the water vapor mixing ratio entering the stratosphere (averaged over the final 3 days of the simulation) versus the peak vertical wind speed. For peak vertical wind speeds less than about 1 cm s^{-1}, the ice crystal number density is still too low to reduce RHI substantially below RHI_{nuc}, so the mixing ratio entering the stratosphere is essentially independent of w. For larger values of w, enough ice crystals nucleate such that crystal growth starts to reduce the RHI well below RHI_{nuc} toward 100%. However, in these simulations a cloud cycle was established: When RHI reaches RHI_{nuc}, ice crystals are nucleated. The crystals rapidly grow and reduce RHI below RHI_{nuc} (shutting off further ice nucleation), eventually driving the RHI down to near 100%. Then the crystals fall out and the RHI builds up again, eventually reaching RHI_{nuc} and triggering another cloud cycle. The period of the cycle is of the order of 1 day. This type of sporadic nucleation has been noted in past modeling studies [e.g., *Sassen and Dodd,* 1989]. The net effect is that the average H_2O mixing ratio entering the stratosphere falls somewhere between the tropopause saturation mixing ratio and 1.6 times this value. As we continue to increase the peak vertical wind speed above 10 cm s^{-1}, the ascent rate approaches and exceeds the crystal fall speed. In these simulations, the ice crystals are advected into the stratosphere and eventually sublimate at temperatures well above the tropopause temperature. As a result, the water vapor mixing ratio above the tropopause is in excess of 5.5 ppmv.

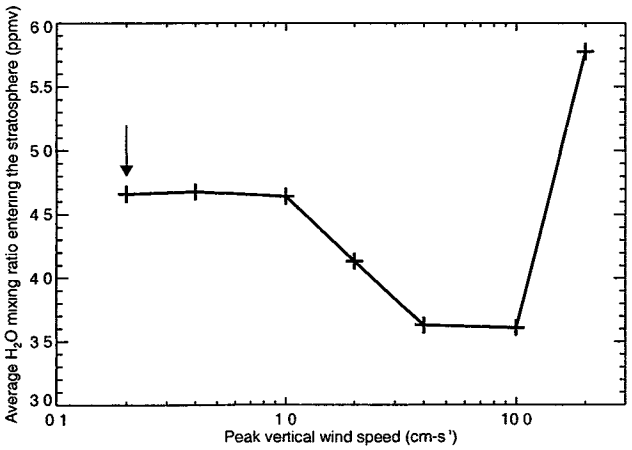

Figure 2. Water vapor mixing ratio just above the tropopause averaged over the final 3 hours of the simulation is plotted versus peak vertical wind speed. The arror indicates the vertical wind speed in balance with clear-sky radiation. See text for discussion.

The actual ice supersaturation required for ice nucleation in the tropical tropopause region is not well known. The value of RHI_{nuc} depends upon the presence of substances other than sulfuric acid in the aerosols. Nitric acid or ammonia may alter the aerosol freezing properties [*Tabazadeh and Toon,* 1998; *Tabazadeh et al.,* 2000], and insoluble components in the aerosols such as mineral particles, soot particles, or precipitated salt crystals would act as heterogeneous freezing sites, thus reducing RHI_{nuc} [*DeMott et al.,* 1997]. *Murphy et al.* [1998] showed that many aerosols near the tropical tropopause are not pure sulfuric acid. Hence, the actual ice supersaturation required for nucleation on the most effective nuclei may be much lower than that required for freezing of sulfuric acid aerosols.

To evaluate the impact of variations in RHI_{nuc} on the potential for dehydration, we have run several simulations with RHI_{nuc} ranging from 110 to 160%. The results are listed in Table 1 and plotted in Figure 3. The ice crystal number density reached in the simulations increases rapidly with decreasing RHI_{nuc}. When the first few crystals nucleate at higher supersaturation, these crystals grow more rapidly and quickly deplete the vapor before more aerosols can freeze. Even for the lowest RHI_{nuc} values used, the ice number density remains relatively low ($< 100\ L^{-1}$), and the ice clouds dehydrate the air to values only slightly below RHI_{nuc}. Hence, the water vapor mixing ratio stratospheric entry value increases approximately linearly with RHI_{nuc}. For the range of RHI_{nuc} considered (110–160%), the water vapor mixing ratio entering the stratosphere ranges from about 3.3 to 4.6 ppmv. The corresponding range in tropopause temperature (assuming air had to cross the tropopause at the saturation mixing ratio) would be –84° to –82.3°C.

The peak optical depth decreases rapidly with increasing RHI_{nuc}, primarily due to the decreasing ice number density. However, even for very small values of RHI_{nuc}, the clouds formed always remain too optically thin to be visible from the ground. The range of optical depths calculated in these simulations is typical of the laminar cirrus observed near the tropopause during the Central Equatorial Pacific Experiment (CEPEX) [*McFarquhar et al.,* 2000].

3. Influence of Waves on the Freeze-Drying Process

It is no doubt unrealistic to assume that ascent across the tropopause occurs purely at a slow, steady rate. Wave motions with a wide range of temporal and spatial scales have been observed near the tropical tropopause. These waves include small-scale disturbances driven by Kelvin-Helmholtz instabilities with periods less than 10 min [*Pfister et al.,* 1986], gravity waves with periods ranging from hours to days [*Pfister et al.,* 1993; *Karoly et al.,* 1996], and Kelvin waves with periods of weeks [*Tsuda et al.,* 1994]. Peak-to-peak vertical parcel excursions in these waves are typically of the order of a few hundred meters. The important influence of the waves on the processes under consideration here is the oscillation in temperature and relative humidity with time. In particular, since the vertical motion and cooling that balance the mean radiative heating are very small (≤ 0.6 cm s^{-1}), waves with vertical wind speed amplitudes of 0.5 cm s^{-1} or larger will drive substantial local enhancements in cooling rate.

Investigation of the impact of the gravity waves on the cloud structure and dehydration process requires multidimensional simulations. For this purpose, we have run 2-D simulations with a horizontal domain large enough to encompass one cycle of the gravity wave, and periodic horizontal boundary conditions. Based on the ER-2 measurements of gravity wave signatures in time-series of wind speed and temperature [*Pfister et al.,* 1986, 1993], we have run simulations with periods of 2 and 24 hours. Gravity wave perturbations in vertical and horizontal wind speed are specified using the expressions given by *Gill* [1982]:

$$w' = w\cos(kx + mz - \omega t), \quad (1)$$

$$u' = -w\frac{m}{k}\cos(kx + mz - \omega t), \quad (2)$$

where w is the vertical wind speed amplitude; k and m are the horizontal and vertical wavenumbers, respectively; and ω is the wave frequency. The horizontal wavelengths used in the 2- and 24-hour simulations are 50 km and 500 km, respectively. The vertical wavelength is 2.2 km. Since we are only concerned with

Table 1. Dehydration Sensitivity to RHI_{nuc}

Simulation Notes	RHI_{nuc}, %	N_{ice}^{max}, L^{-1}	r_{eff}, μm	τ_{max}	H_2O,[a] ppmv
No ice nucleation	N.A.[b]	N.A.	N.A.	N.A.	>6
	110	28	8–14	0.0036	3 33
	120	3.5	12–16	0.00091	3.56
	130	1.1	13–17	0.00056	3.88
	140	0 51	14–17	0.00036	4.16
	150	0.26	15–18	0.00021	4.45
Baseline	158	0.15	15–18	0.00012	4.69 7

[a]Stratospheric entry value.
[b]N.A denotes not applicable.

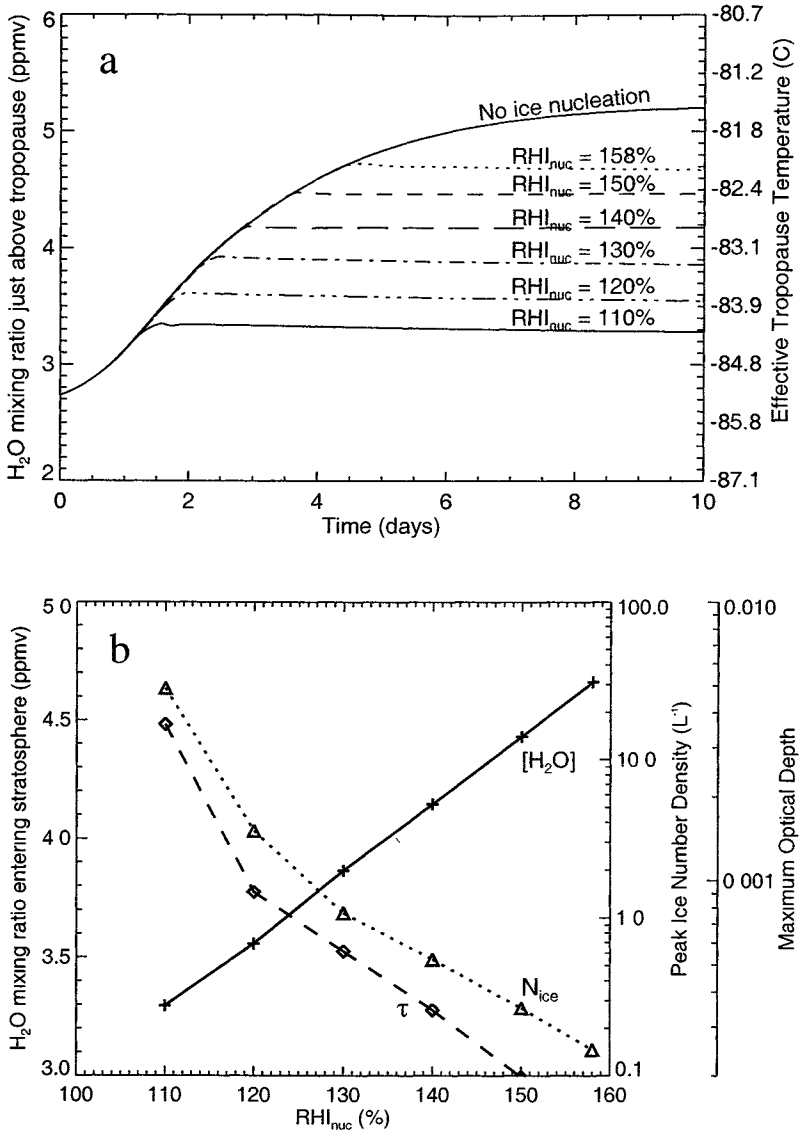

Figure 3. (a) The evolution of water vapor mixing ratio 100 m above the tropopause is plotted versus time for simulations with no ice nucleation and various values of RHI_{nuc}. The right axis shows the tropopause temperatures such that the saturation mixing ratio would equal the H_2O mixing ratios on the left axis. (b) Summary of results from simulations using a range of values for the threshold relative humidity with respect to ice (RHI_{nuc}). The water vapor mixing ratio just above the tropopause (solid line), the peak ice number density (dotted line), and the maximum cloud visible optical depth (dashed line) are plotted versus RHI_{nuc}.

the effects of the wave in a narrow vertical region near the tropopause, the vertical variations in wavenumber and amplitude are not important for this study. A vertical wind speed amplitude of 10 cm s^{-1} is used for the 2-hour wave simulation, and an order of magnitude smaller amplitude is used in the 24-hour wave case such that the vertical displacement amplitudes of the waves are approximately equal. The wave amplitude is allowed to build up linearly with time during the first 4 and 48 hours of the 2-hour wave and 24-hour wave simulations, respectively.

A time step of 100 s is used for the transport calculations. Smaller substeps are used for the microphysics calculations. A variable time-step is used for the microphysics calculations: The microphysics substep size is determined such that particle concentrations do not change by more than 20% during the time step. This scheme results in many microphysics substeps being taken within a particular dynamics time step when rapid microphysical processes such as ice nucleation occur. The horizontal grid sizes are 50 m and 500 m in the 2-hour and 24-hour wave simulations, respectively.

Plate 3 shows the vertical wind speed pattern in the 2-D domain at 15 hours in the 2-hour wave simulation. A wave pattern is apparent with an amplitude of about 10 cm s^{-1} and a vertical wavelength of 2.2

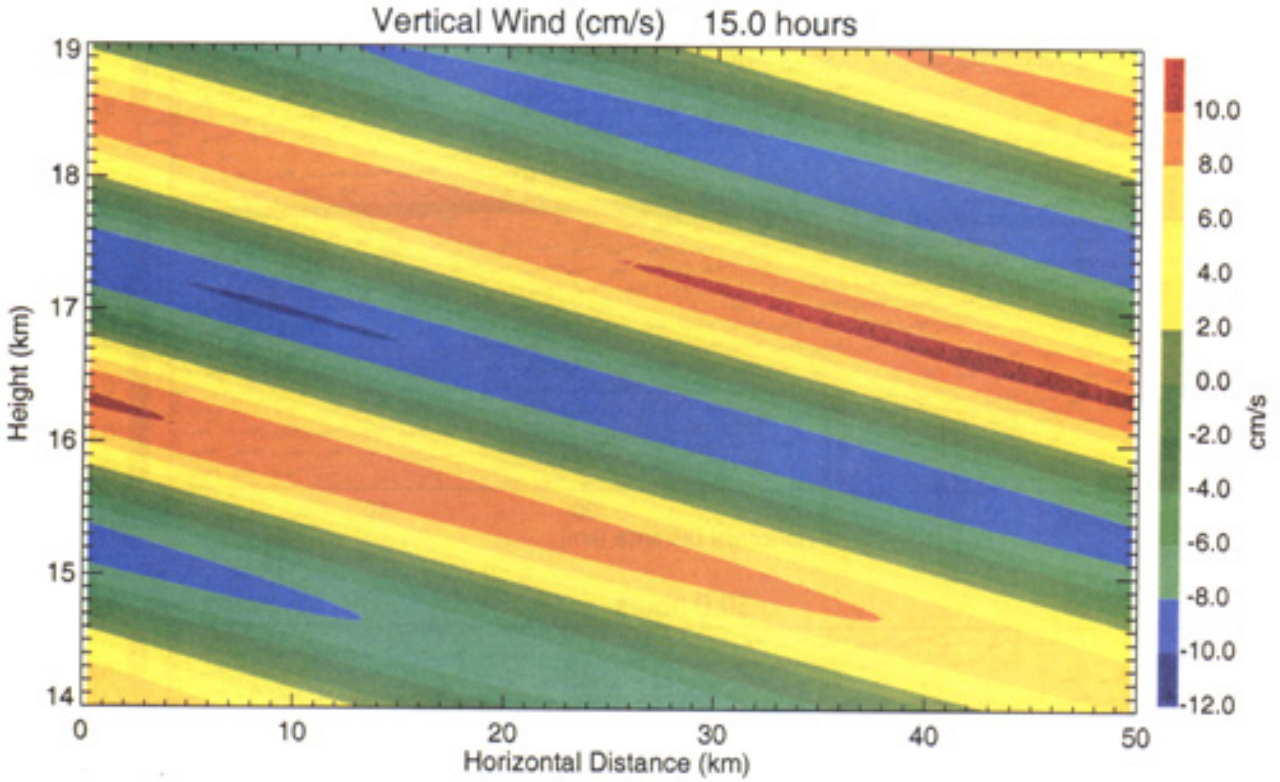

Plate 3. The vertical wind speed is shown versus horizontal and vertical distance at 15 hours into the simulation with a 2-hour oscillating forcing at the lower boundary. A gravity wave pattern is evident with a vertical wavelength of about 2.2 km.

km. The resulting peak-to-peak amplitude of the temperature oscillation is about 2–3 K. This amplitude is consistent with gravity wave temperature oscillations observed with the ER-2 (typically 1–6 K peak-to-peak) [*Pfister et al.,* 1986, 1993, 2001]. Note that we are also imposing a slow rising mean motion in balance with the radiative heating as in our 1-D simulations described above.

The cloud ice water content at three times in the 2-hour wave simulation is shown in Plate 4. The wave perturbation in temperature causes a horizontal relative humidity variation of about 30–40%. Ice nucleation occurs first at the coldest point in the wave when the RHI reaches RHI_{nuc} (about 160% in this case). Even with the increased cooling rate due to the gravity wave, the ice number densities in the cloud are still very low ($< 2\ L^{-1}$) due to the high threshold for ice nucleation. Since the wave oscillation is not sufficient to drive the air parcels below ice saturation (RHI=100%), the ice crystals do not sublimate in the warmer phase of the wave, and about one wave period (2 hours) after the initial ice nucleation, ice crystals are present across the entire horizontal wavelength. The primary effect of this high-frequency wave on the cloud structure is to cause an undulation in the cloud layer. In simulations with larger wave amplitudes, the air is subsaturated in the warm phase of the wave, so ice is only present at the cold wave crests. As in our baseline simulation without waves, the ice nucleation and growth prevents the humidity of air crossing the tropopause from exceeding RHI_{nuc}, but the crystals sediment out before the RHI is decreased very far below RHI_{nuc}.

Given the larger horizontal wavelength and smaller heating amplitude used in the 24-hour wave simulation, the resulting vertical wind speed field develops a pattern very similar to that shown in Plate 3, except that the wind speeds are about an order of magnitude smaller. Plate 5 shows the cloud structure at three times in the 24-hour wave simulation (again using $RHI_{nuc} = 160\%$). In this case, the gravity wave has a large impact on the cloud structure. Similar to laminar cirrus observed during the Tropical Ozone Transport Experiment - Vortex Ozone Transport experiment [*Pfister et al.,* 2001], the cloud is tilted by the wave. Ice crystals are nucleated sporadically at the crest of the wave (where RHI is highest). These crystals grow and fall out of the supersaturated layer within several hours; hence, in the warmest phase of the wave, little or no ice remains. Note that the horizontal/vertical aspect ratio of Plate 5 is 10 times larger than Plate 4. The clouds actually have very high horizontal/vertical aspect ratios in both simulations.

The impact of the waves in these simulations on the water vapor mixing ratio of air entering the stratosphere is shown in Figure 4. Even though the wave motions are

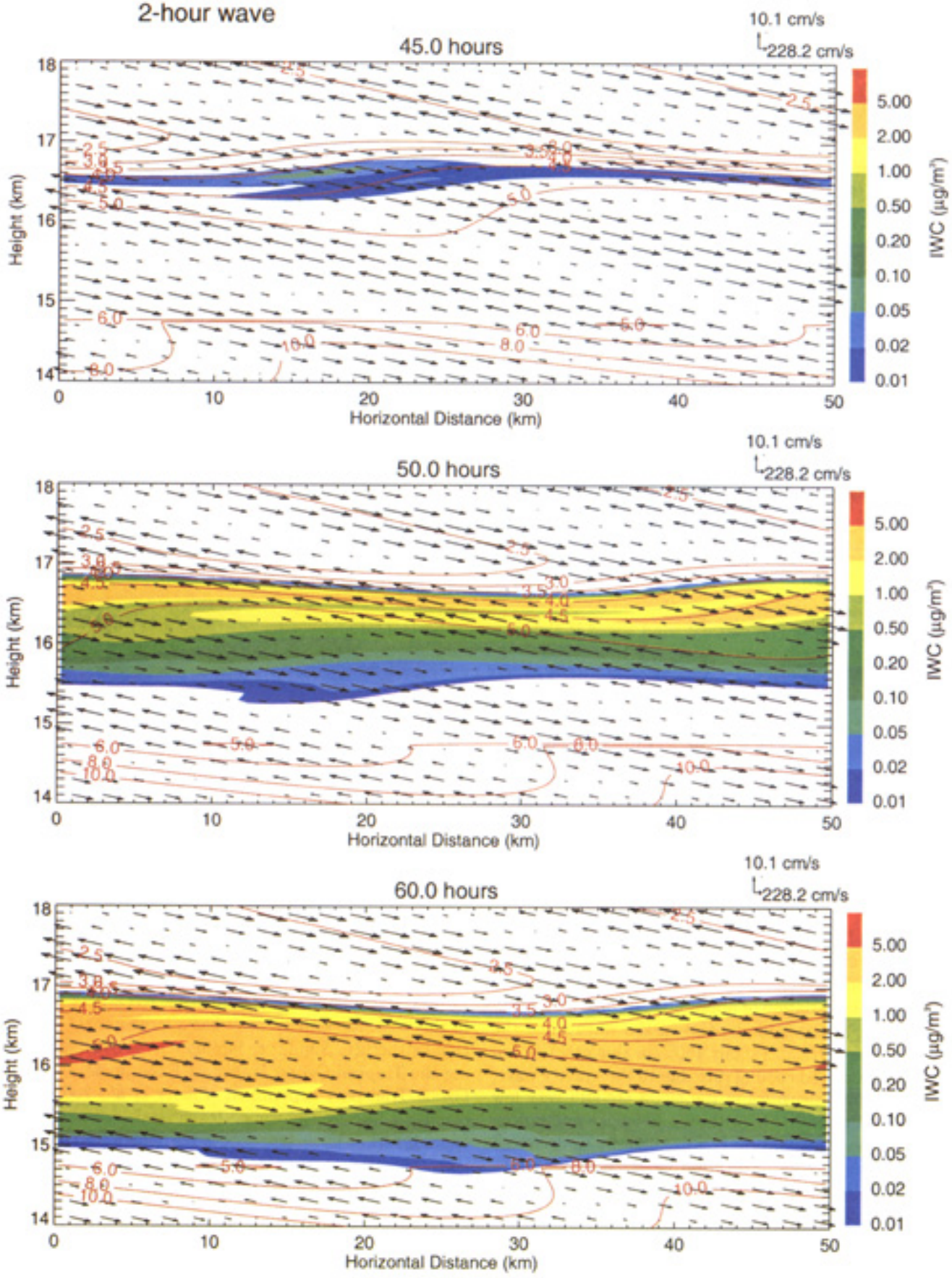

Plate 4. Cloud ice water content (IWC, color shading), water vapor mixing ratio (red contours), and wind speed (arrows) are plotted versus horizontal and vertical distance at 45, 50, and 60 hours in the 2-hour wave simulation. Cause an undulation in the cloud layer, but ice crystals are present across the entire wavelength.

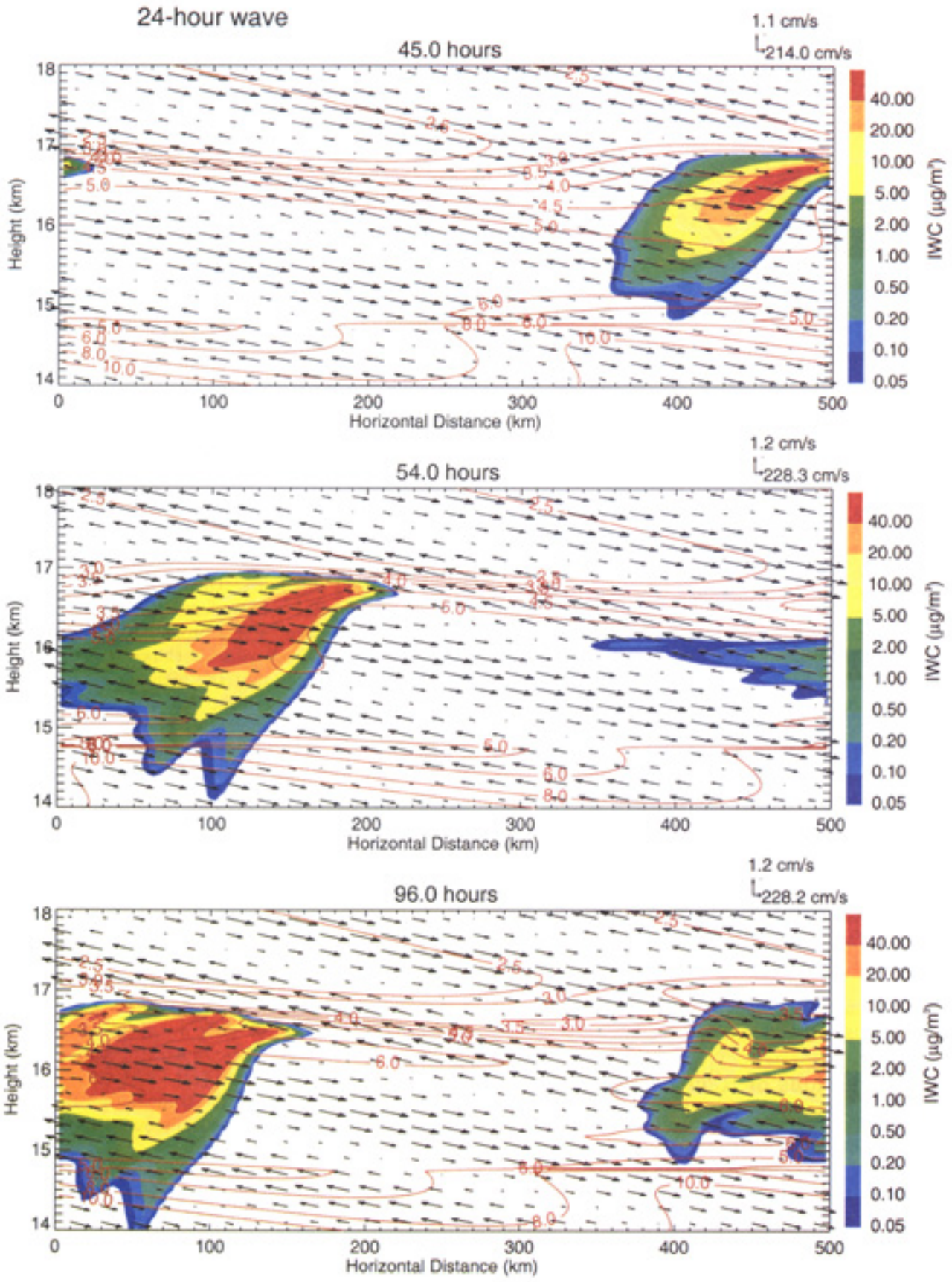

Plate 5. Same as Plate 4, but at 45, 54, and 90 hours in the 24-hour wave simulation.

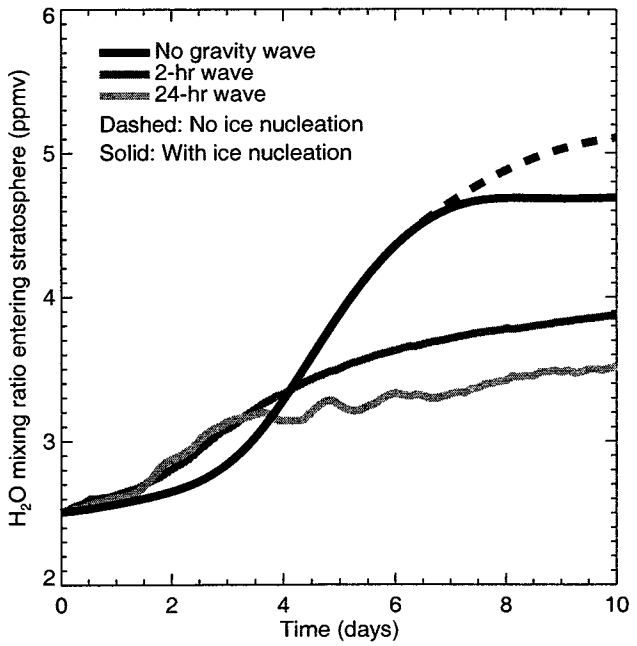

Figure 4. The horizontally averaged water vapor mixing ratio just above the tropopause is plotted versus time for simulations without waves, and with 24- and 2-hour waves. In the simulations with gravity waves, the mixing ratio is controlled by the minimum temperature in the wave, which is colder than the mean tropopause temperature. Hence, the air is dehydrated to lower water vapor mixing ratios with wave-driven temperature oscillations than without waves.

insufficient to generate large ice number densities (and rapid depletion of water vapor in excess of saturation), they do result in considerable reductions in the flux of water into the stratosphere. The cause of this reduction is that air parcels entering the stratosphere through the gravity wave have their water vapor mixing ratios limited to $(RHI_{nuc}/100)$ times the saturation mixing ratio corresponding to the gravity wave minimum temperature. Since the minimum temperature in the wave is 1–2 K lower than the mean tropopause temperature, less water passes through the tropopause when the waves are present. Of course, larger amplitude waves would result in even greater reductions in water vapor mixing ratio entering the stratosphere.

4. Observations of Relative Humidity Near the Tropical Tropopause

The modeling analysis described above suggests that air may remain supersaturated with respect to ice as it rises across the tropopause. This result raises the question of whether supersaturated air has been observed near the tropical tropopause. To address this issue, we have gathered in situ water vapor measurements made with both aircraft-borne and balloon-borne instruments over the past several years. The flight locations, instrumentation, and relevant references are listed in Table 2.

Discrepancies of the order of 10–25% between H_2O measurements made with the National Oceanographic and Atmospheric Administration (NOAA) Lyman α instrument, the Harvard Lyman α instrument, and the cryogenic hygrometers have been documented [*Dessler et al.*, 1995]; to date these discrepancies are not entirely resolved. However, *Hintsa et al.* [1999] recently validated the Harvard Lyman α measurements by painstaking calibration and in-flight comparison with the Jet Propulsion Laboratory diode laser hygrometer. Since the Harvard instrument generally reported higher humidities than the NOAA Lyman α or the cryogenic hygrometers, humidities from the later instruments should perhaps be treated as underestimates. For this analysis, we will simply assume that these water vapor measurements yield absolute relative humidity uncertainties of the order of 10–20%.

Based on these tropical tropopause humidity measurements, we have generated a frequency distribution of RHI measurements within 100 m of the tropopause (Figure 5). The ER-2 measurements were all made during ascent, descent, or in dips so the tropopause location could be estimated from the time series of temperature and altitude measurements. The majority of the measurements indicated tropopause RHI values between about 60 and 100%. Of the 40 profiles, only 6 indicated tropopause relative humidities well above ice saturation. An example of a profile indicating supersaturation at the tropopause is shown in Figure 6a. It is difficult to argue that the high supersaturations were a result of measurement bias in a particular instrument since highly supersaturated conditions at the tropopause were detected in particular profiles with all of the water vapor instruments used in the different experiments (see Table 2). However, it is important to remember that accurate calculation of humidity requires very accurate temperature measurements. An error in the ambient temperature (or frost point temperature for the cryogenic hygrometer) measurement of about 1 K would result in an RHI error of about 20%. Also, during some of these measurements, cirrus were present. Ice crystals may have entered the instruments and sublimated, resulting in anomalously high water vapor mixing ratio measurements. Given the small number of observations and the difficulty of accurately measuring relative humidity, these supersaturation observations provide only limited support for the existence of supersaturated air crossing the tropopause. However, the observations certainly do not discount this possibility.

The data also indicate that the humidity at the tropopause is often well below ice saturation. One of these relatively dry profiles is shown in Figure 6b. If we assume that humid air is injected into the upper troposphere by deep convection and this air subsequently rises slowly across the tropopause, then the RHI at the tropopause should be near (or above) saturation. Air parcels likely cross the tropopause on trajectories only

Table 2. In Situ RHI Measurements

Experiment[a]	Instrument	Date	Latitude, Longitude	z_{trop}	T_{trop}	RHI[b]	RHI_{max}[c]
STEP	NOAA Lyman α[d]	Jan 13, 1987	10°S, 140°E	16.98	-89.2	124–170	170
STEP	NOAA Lyman α[d]	Jan 18, 1987	10°S, 140°E	16 29	-84 0	70–91	95
STEP	NOAA Lyman α[d]	Jan. 22, 1987	10°S, 140°E	16 51	-85.4	79–102	147
STEP	NOAA Lyman α[d]	Jan. 23, 1987	10°S, 140°E	16.52	-84.5	91–109	142
STEP	NOAA Lyman α[d]	Jan 29, 1987	10°S, 140°E	16 38	-84.2	52–75	96
STEP	NOAA Lyman α[d]	Jan. 31, 1987	10°S, 140°E	16.64	-83.3	65–69	122
STEP	NOAA Lyman α[d]	Feb 2, 1987	10°S, 140°E	16.84	-85.8	68–98	146
STEP	NOAA Lyman α[d]	Feb 3, 1987	10°S, 140°E	16.97	-83.5	64–77	94
STEP	NOAA Lyman α[d]	Feb. 8, 1987	10°S, 140°E	16 25	-84.5	90–101	100
STEP	NOAA Lyman α[d]	Feb 12, 1987	10°S, 140°E	16.81	-83.9	62–81	95
AAOE	NOAA Lyman α[d]	Aug. 12, 1987	10°N, 85°W	15.72	-79.9	58–72	116
CEPEX	Cryogenic[e]	March 7, 1993	9°S, 160°E	16 68	-90.1	35–76	93
CEPEX	Cryogenic[e]	March 12, 1993	2°S, 179°E	17 63	-89 3	140–141	147
CEPEX	Cryogenic[e]	March 13, 1993	2°S, 178°W	17.31	-87 5	67–75	129
CEPEX	Cryogenic[e]	March 13, 1993	2°S, 175°W	17 50	-86 8	87–102	101
CEPEX	Cryogenic[e]	March 14, 1993	2°S, 171°W	16 84	-87 2	88–109	109
CEPEX	Cryogenic[e]	March 15, 1993	2°S, 167°W	17.28	-83 8	44–66	84
CEPEX	Cryogenic[e]	March 16, 1993	2°S, 163°W	17 00	-83 6	48–51	63
CEPEX	Cryogenic[e]	March 17, 1993	1°S, 159°W	17 24	-84.7	51–73	73
CEPEX	Cryogenic[e]	March 20, 1993	2°N, 157°W	16.94	-81.1	68–94	98
CEPEX	Cryogenic[e]	March 22, 1993	2°N, 157°W	17 35	-79.6	32–44	115
CEPEX	Cryogenic[e]	March 24, 1993	2°N, 157°W	15 84	-80 9	103–141	141
CEPEX	Cryogenic[e]	March 24, 1993	2°N, 157°W	16 05	-79 1	61–78	91
CEPEX	Cryogenic[e]	March 26, 1993	2°N, 157°W	17 56	-79.5	34–39	67
ASHOE	NOAA Lyman α[d]	March 21, 1994	0°N, 158°W	17 3	-78 7	33–43	48
ASHOE	NOAA Lyman α[d]	March 22, 1994	7°S, 159°W	16 4	-79 5	41–48	48
ASHOE	NOAA Lyman α[d]	March 22, 1994	11°S, 159°W	15 7	-77 6	50–66	68
ASHOE	NOAA Lyman α[d]	Oct 26, 1994	1°N, 159°W	17 3	-85 5	112–119	129
ASHOE	NOAA Lyman α[d]	Oct. 29, 1994	1°S, 159°W	16 2	-83 1	74–82	87
STRAT	Harvard Lyman α[f]	Nov. 5, 1995	1°N, 160°W	17 4	-82 1	91–100	100
STRAT	Harvard Lyman α[f]	Nov 5, 1995	2°N, 160°W	17 5	-83.8	119–132	132
STRAT	Harvard Lyman α[f]	Feb 13, 1996	0°N, 155°W	16 6	-86 2	79–109	113
STRAT	Harvard Lyman α[f]	Feb 13, 1996	1°N, 155°W	16.6	-86.9	76–106	110
STRAT	Harvard Lyman α[f]	Aug 1, 1996	1°N, 159°W	16.7	-82 5	96–98	102
STRAT	Harvard Lyman α[f]	Aug. 1, 1996	1°N, 159°W	16.8	-82.7	77–106	106
STRAT	Harvard Lyman α[f]	Aug 8, 1996	6°N, 155°W	17.0	-77.4	36–64	64
STRAT	Harvard Lyman α[f]	Aug. 8, 1996	8°N, 156°W	16.6	-77.5	54–64	79
STRAT	Harvard Lyman α[f]	Dec. 11, 1996	1°N, 155°W	17.4	-87.1	106–129	141
POLARIS	Harvard Lyman α[f]	Sep. 23, 1997	2°S, 159°W	17.6	-76.9	36–46	59
POLARIS	Harvard Lyman α[f]	Sep. 23, 1997	0°S, 159°W	17.8	-79.6	61–69	69

[a]Experiments are as follows: Stratosphere-Troposphere Exchange Project (STEP), Airborne Antarctic Ozone Experiment (AAOE), Central Equatorial Pacific Experiment (CEPEX), Airborne Southern Hemisphere Ozone Experiment (ASHOE), Stratospheric Tracers of Atmospheric Transport (STRAT), and Photochemistry of Ozone Loss in the Arctic Region in Summer (POLARIS).

[b]Range within 100 m of the tropopause is given.

[c]Maximum RHI in the 15–19 km height range.

[d]See *Kelly et al.* [1993] for instrument details.

[e]See *Oltmans and Hofmann* [1995] for instrument details and *Kley et al.* [1996] for description of CEPEX measurements.

[f]See *Weinstock et al.* [1994] for instrument details.

slightly inclined from horizontal; hence, it is possible that the temperature minimum in a particular balloon or aircraft profile is not the point where air parcels reached their minimum temperature. The right column in Table 2 indicates that the profiles usually included RHI values near 100% somewhere between 15 and 19 km, but a few profiles were remarkably dry throughout the tropopause region. The source of subsaturated air at the tropical tropopause could be isentropic mixing of dry midlatitude stratospheric air masses into the tropical upper troposphere. Dry air at some locations along the tropopause would also be expected if wave motions were present. As indicated by the simulation with g13'-ity waves described above, in the descending phase of waves, the RHI can be well below 100% even when the mean humidity is near ice saturation.

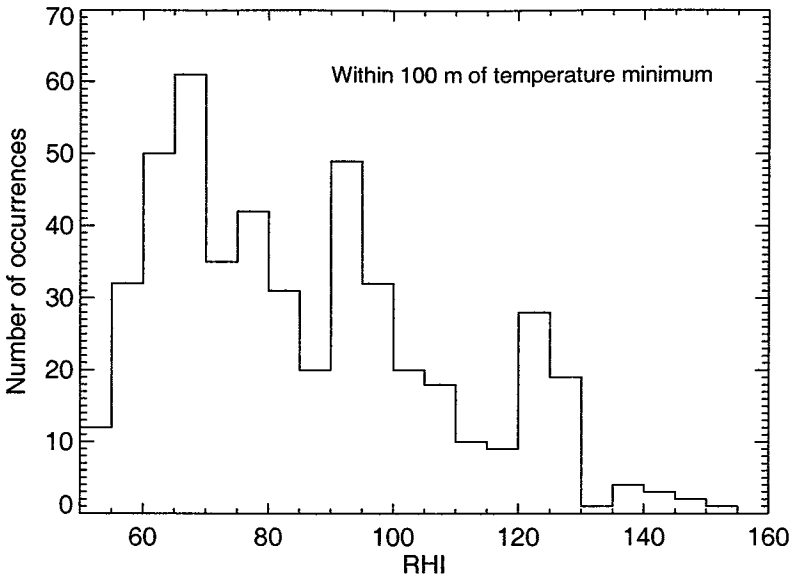

Figure 5. Frequency distribution of 10-second RHI measurements made within 100 m of the tropical tropopause (temperature minimum). The flight locations, instruments, and dates are listed in Table 2.

5. Summary and Discussion

The modeling analysis presented here suggests that if air rises slowly across the tropical tropopause and ice nucleation only occurs in sulfate aerosols, then optically thin clouds with very low ice crystal number densities (0.5–100 L^{-1}) will form near the tropopause. These clouds will freeze-dry the air to within a factor of about 1.6 of the tropopause saturation mixing ratio. As *Rosenfield et al.* [1998] pointed out, the laminar cirrus at the tropopause will also heat the tropopause, effectively allowing larger water vapor mixing ratios to enter the stratosphere; however, if no clouds form as air rises across the tropopause, then unrealistically humid air enters the stratosphere. Hence, we argue that the net effect of the laminar cirrus must be to dehydrate the air.

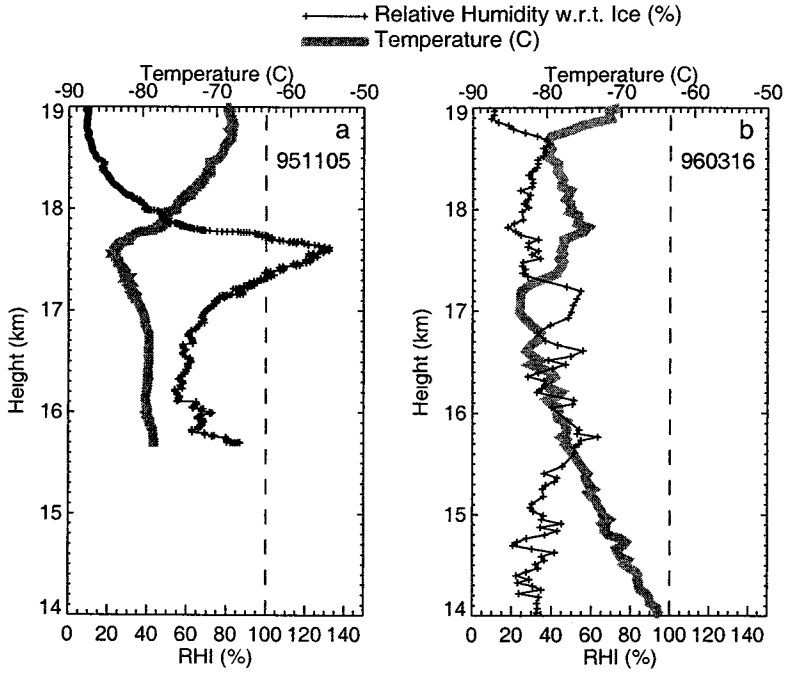

Figure 6. Temperature and RHI profiles from in situ measurements. (a) An example of supersaturated air near the tropopause (ER-2 descent on November 11, 1995), (b) An example of dry air throughout the tropopause region (balloon-borne cryogenic hygrometer profile on March 16, 1993). See Table 2 for details.

The simulations also suggest that the efficiency of dehydration in this rising air increases substantially if effective ice nuclei are present. The water vapor mixing ratio entering the stratosphere can range from 1 to 1.6 times the tropopause saturation mixing ratio, depending upon how effective the ice nuclei are.

We also tested the sensitivity to vertical wind speed with the temperature profile held fixed. As the ascent rate is increased, larger ice crystal number densities are generated. For peak vertical wind speeds less than about 1 cm s^{-1}, the ice crystal number density is still too low to drive the RHI well below RHI_{nuc}, so the water vapor mixing ratio entering the stratosphere is independent of w. If w is increased further, the relative humidity of air entering the stratosphere is driven down toward 100%. However, if w is increased beyond about 10 cm s^{-1}, the ascent rate exceeds the terminal velocity of the ice crystals and no dehydration occurs.

Two-dimensional simulations suggest that temperature oscillations driven by gravity waves can enhance the dehydration. Air entering the stratosphere across the tropopause with gravity waves present will have a lower mixing ratio due to the cold temperature minima in the wave.

With the low ice number densities in these clouds, the number of aerosols contributing to ice nucleation is less than 0.1% of the total aerosol population. Hence, it is possible that a small fraction of the aerosol population act as effective ice nuclei and control the ice nucleation process. For example, a small number of sulfate aerosols containing solid mineral cores might act as effective heterogeneous freezing nuclei. In this case, the composition of aerosols that numerically dominate the aerosol population (presumably sulfate with some amount of organic material) may be irrelevant.

The ice number densities predicted in these simulations are much lower than those reported in our earlier modeling study [*Jensen et al.*, 1996]. The difference arises from two factors: First, in the previous study we were using an ice nucleation parameterization which predicted much lower values of RHI_{nuc}, resulting in higher ice number densities (see Figure 3). Second, in the earlier study, we forced the cloud formation with much higher cooling rates due to gravity wave motions, resulting in higher ice number densities.

In situ water vapor measurements provide some support for our hypothesis that supersaturated air can exist at the tropical tropopause. In addition, the data show that subsaturated air is also often present. These results suggest that assuming air enters the lower stratosphere with H_2O mixing ratio equal to the tropopause saturation mixing ratio is an oversimplification. We are not denying the importance of tropopause temperature in controlling the water vapor mixing ratio entering the stratosphere. Indeed, the seasonal cycle of water vapor concentration in the lower stratosphere is no doubt controlled by the seasonal cycle in tropopause temperature [*Weinstock et al.*, 1995]. However, quantitative analysis of the stratospheric entry H_2O mixing ratio to within a few tenths of a parts per million per volume will require a detailed understanding of the dynamical and microphysical processes occurring near the tropopause.

This analysis is speculative, primarily due to the scarcity of measurements made in the tropical tropopause region. In situ measurements from flights along the tropopause would be particularly useful. Accurate measurements of water vapor, temperature, vertical wind speed, ice crystal size distributions, and ice nuclei would provide a much clearer understanding of the dehydration process.

Acknowledgments. This research was supported by both NASA's Upper Atmospheric Research Satellite Interdisciplinary Research Program, directed by Joe McNeal, and NASA's Stratospheric Aerosol and Gas Experiment, directed by Phil DeCola We appreciate the data and assistance provided by Ken Kelley, Sam Oltmans, Elliot Weinstock, and Paul Bui.

References

Brewer, A M., Evidence for a world circulation provided by the measurements of helium and water vapor distribution in the stratosphere, *Q. J. R. Meteorol. Soc., 75*, 351–363, 1949

Brock, C A., P. Hamill, J. C. Wilson, H. H. Jonsson, and K. R Chan, Particle formation in the upper tropical troposphere: A source of nuclei for the stratospheric aerosol, *Science, 270*, 1650–1653, 1995.

Clarke, A D., Atmospheric nuclei in the remote free troposphere, *J. Atmos. Chem., 14*, 479–488, 1992.

Clough, S. A , M. J. Iacono, and J.-L. Moncet, Line-by-line calculations of atmospheric fluxes and cooling rates: Application to water vapor, *J. Geophys. Res., 97*, 15,761–15,785, 1992.

Danielsen, E. F., In situ evidence of rapid, vertical, irreversible transport of lower tropospheric air into the lower tropical stratosphere by convective cloud turrets and by larger-scale upwelling in tropical cyclones, *J. Geophys. Res., 98*, 8665–8681, 1993.

DeMott, P. J., D C. Rogers, and S. M Kreidenweis, The susceptibility of ice formation in upper tropospheric clouds to insoluble aerosol components, *J. Geophys. Res., 102*, 19,575–19,584, 1997.

Dessler, A., reexamination of the "stratospheric fountain hypothesis," *Geophys. Res. Lett., 25*, 4165–4168, 1998

Dessler, A. E , E J Hintsa, E. M. Weinstock, J G Anderson, and K. R Chan, Mechanisms controlling water vapor in the lower stratosphere: "A tale of two stratospheres", *J. Geophys. Res., 100*, 23,167–23,172, 1995

Gierens, K , U Schumann, M. Helten, H. Smit, and A. Marenco, A distribution law for relative humidity in the upper troposphere and lower stratosphere derived from three years of MOZAIC measurements, *Ann. Geophys., 17*, 1218–1226, 1999

Gill, A. E , *Atmosphere-Ocean Dynamics*, Academic, San Diego, Calif., 1982.

Hamill, P , O. B. Toon, and C. S. Kiang, Microphysical processes affecting stratospheric aerosol particles, *J. Atmos. Sci., 34*, 1104–1119, 1977

Heymsfield, A J., L M. Miloshevich, C. Twohy, G Sachse, and S Oltmans, Upper tropospheric relative humidity observations and implications for cirrus ice nucleation, *Geophys. Res. Lett., 25*, 1343–1346, 1998

Hintsa, E J , E M. Weinstock, J G Anderson, R. D May, and D F. Hurst, On the accuracy of in situ water vapor measurements in the troposphere and lower stratosphere

with the Harvard Lyman α hygrometer, *J. Geophys. Res., 104*, 8183–8189, 1999.

Jensen, E. J., and O. B Toon, Ice nucleation in the upper troposphere: Sensitivity to aerosol number density, temperature, and cooling rate, *Geophys. Res. Lett., 21*, 2019–2022, 1994

Jensen, E J , O B Toon, D L. Westphal, S Kinne, and A J. Heymsfield, Microphysical modeling of cirrus part I: Comparison with 1986 FIRE IFO measurements, *J. Geophys. Res., 99*, 10,421–10,422, 1994

Jensen, E J., O B Toon, L Pfister, and H. B. Selkirk, Dehydration of the upper troposphere and lower stratosphere by subvisible cirrus clouds near the tropical tropopause, *Geophys. Res. Lett., 23*, 825–828, 1996

Jensen, E J , et al., Ice nucleation in upper tropospheric wave-clouds observed during SUCCESS, *Geophys. Res. Lett., 25*, 1363–1366, 1998a

Jensen, E. J , A S Ackerman, D. E Stevens, O. B Toon, and P Minnis, Spreading and growth of contrails in a sheared environment, *J. Geophys. Res., 103*, 31,557–31,569, 1998b

Jensen, E J., W. G. Read, J Merganthaler, B. J Sandor, L. Pfister, and A. Tabazadeh, High humidities and subvisible cirrus near the tropical tropopause, *Geophys. Res. Lett., 26*, 2347-2350, 1999

Karoly, D. J , G. L. Roff, and M. J. Reeder, Gravity wave activity associated with tropical convection detected in TOGA COARE sounding data, *Geophys. Res. Lett., 23*, 261–264, 1996.

Kelly, K. K , M H Proffitt, K. R Chan, M Loewenstein, J. R. Podolske, S E. Strahan, J. C. Wilson, and D Kley, Water vapor and cloud water measurements over Darwin during the STEP 1987 Tropical mission, *J. Geophys. Res., 98*, 8713–8723, 1993

Kley, D., et al., Observations of near-zero ozone concentrations over the convective Pacific: Effects on air chemistry, *Science, 274*, 230–233, 1996

Koop, T , H. P. Ng, L. T. Molina, and M J. Molina, A new optical technique to study aerosol phase transitions: The nucleation of ice from H_2SO_4 aerosols, *J. Phys. Chem., 102*, 8924, 1998.

McFarquhar, G M , A. J Heymsfield, J Spinhirne, and B Hart, Thin and subvisual tropopause cirrus: Observations and radiative impacts, *J. Atmos. Sci , 57*, 1841–1853, 1999.

Murphy, D M , D S Thomson, and M J Mahoney, In situ measurements of organics, meteoritic material, mercury, and other elements in aerosols at 5 to 19 kilometers, *Science, 282*, 1664–1669, 1998

Newell, R E , and S Gould-Stewart, A stratospheric fountain?, *J. Atmos. Sci., 38*, 2789–2796, 1981.

Oltmans, S J , and D J. Hofmann, Increase in lower stratospheric water vapour at a mid-latitude Northern Hemisphere site from 1981 to 1994, *Nature, 374*, 146–149, 1995

Pfister, L , W. Starr, R. Craig, M. Loewenstein, and M Legg, Small-scale motions observed by aircraft in the tropical lower stratosphere: Evidence for mixing and its relationship to large-scale flows, *J. Atmos. Sci., 43*, 3210–3225, 1986

Pfister, L , K. R. Chan, T P Bui, S. Bowen, M Legg, B Gary, K Kelly, M Proffitt, and W. Starr, Gravity waves generated by a tropical cyclone during the STEP tropical field program: A case study, *J Geophys. Res., 98*, 8611–8589, 1993

Pfister, L , H B Selkirk, E. J. Jensen, M R. Schoeberl, O B. Toon, E. V. Browell, W B. Grant, B Gary, M J. Mahoney, T V Bui, E Hintsa, Aircraft observations of thin cirrus clouds near the tropical tropopause, *J. Geophys. Res., 106*, 9765–9786, 2001

Robinson, G. D , The transport of minor atmospheric constituents between the troposphere and stratosphere, *Quart. J Roy. Meteor. Soc., 106*, 227, 1980

Rosenfield, et al , The impact of subvisible cirrus clouds near the tropical tropopause on stratospheric water vapor, *Geophys. Res. Lett., , 25*, 1883–1886, 1998.

Russell, P B , L Pfister, and H B. Selkirk, The tropical experiment of the Stratosphere-Troposphere Exchange Project (STEP): Science objectives, operations, and summary findings, *J. Geophys. Res., 98*, 8563, 1993.

Sassen, K , and G C. Dodd, Haze particle nucleation simulations in cirrus clouds, and applications for numerical and lidar studies, *J. Atmos. Sci., 46*, 3005, 1989.

Sassen, K., M K. Griffin, and G. C. Dodd, Optical scattering and microphysical properties of subvisible cirrus clouds, and climatic implications, *J. Appl. Meteorol., 28*, 91–98, 1989.

Solomon, S., R R. Garcia, F. S. Rowland, and D. J. Wuebbles, On the depletion of Antarctic ozone, *Nature, 321*, 755–758, 1986

Tabazadeh, A., and O. B. Toon, The role of ammoniated aerosols in cirrus cloud nucleation, *Geophys. Res. Lett., 25*, 1379–1383, 1998.

Tabazadeh, A , S. T. Martin, and J -S Lin, The effect of particle size and nitric acid uptake on the homogeneous freezing of aqueous sulfuric acid particles, *Geophys. Res. Lett., 27*, 1111–1115, 2000.

Toon, O B., R. P. Turco, J. Jordan, J. Goodman, and G. Ferry, Physical processes in polar stratospheric ice clouds, *J. Geophys. Res., 94*, 11,359–11,380, 1989a.

Toon, O B., C. P McKay, T. P Ackerman, and K. Santhanam, Rapid calculation of radiative heating rates and photodissociation rates in inhomogeneous multiple scattering atmospheres, *J. Geophys. Res., 94*, 16,287–16,301, 1989b

Tsuda, T , Y Murayama, H Wiryosumarto, S Woro, B. Harijono, and S Kato, Radiosonde observations of equatorial atmosphere dynamics over Indonesia, 1, Equatorial waves and diurnal tides, *J. Geophys. Res., 99*, 10,491–10,505, 1994

Wang, P -H , P Minnis, M P McCormick, G S Kent, and K M Skeens, A 6-year climatology of cloud occurrence frequency from Stratospheric Aerosol and Gas Experiment II observations (1985–1990), *J. Geophys. Res., 101*, 29,407–29,429, 1996.

Weinstock, E. M , E J. Hintsa, A E Dessler, J. F. Oliver, N L Hazen, J N Demusz, N T Allen, L B Lapson, and J G Anderson, New fast response photofragment fluorescence hygrometer for use on the NASA ER-2 and the Perseus remotely piloted aircraft, *Rev. Sci. Instrum., 65*, 3544–3554, 1994.

Weinstock, E M., E. J Hintsa, A E. Dessler, and J G. Anderson, Measurements of water vapor in the tropical lower stratosphere during the CEPEX campaign: Results and interpretation, *Geophys. Res. Lett., 22*, 3231–3234, 1995

Winker, D M , and C R. Trepte, Laminar cirrus observed near the tropical tropopause by LITE, *Geophys. Res. Lett. 25*, 3351–3354, 1998

A S Ackerman, E J Jensen, L. Pfister, and A Tabazadeh, NASA Ames Research Center, MS 245-4, Moffett Field, CA 94035 (ejensen@sky arc.nasa.gov)

O B Toon, University of Colorado, Laboratory for Atmospheric and Space Physics, Campus Box 392, Boulder, CO, 80309 (toon@lasp.colorado edu)

(Received February 3, 2000; revised July 25, 2000; accepted August 28, 2000.)